Meteorol Atmos Phys 81, 67–83 (2002)

Meteorology and Atmospheric Physics

[1] Key Laboratory for Mesoscale Severe Weather of Ministry of Education, Nanjing University, Nanjing, China
[2] Department of Earth Science, Nanjing University, Nanjing, China
[3] Cold and Arid Regions Environmental and Engineering Research Institute, Lanzhou, China

The effects of land-surface heterogeneities on regional climate: A sensitivity study

X.-M. Zeng[1,2], **M. Zhao**[1], **B.-K. Su**[1], **J.-P. Tang**[1], **Y.-Q. Zheng**[1], **Y.-J. Zhang**[3], and **J. Chen**[2]

With 6 Figures

Received June 19, 2001
Revised January 21, 2002

Summary

In order to further understand the land–atmosphere interactions and increase the predictability of climate models, it is very important to investigate the effects of land-surface heterogeneities. In this paper, we considered roughness-length and stomatal-resistance heterogeneities in the regional climate model RegCM2 (Giorgi et al, 1993) that employs BATS (Dickinson et al, 1993) as the land surface scheme. In representing the subgrid heterogeneities, a computationally efficient method, which is a combination of the mosaic approach and the analytical type of the statistical-dynamical approach, is applied. The method is also characterized by converting the probability distribution of fundamental variables to probability distributions of derived quantities. By using the 3-month observational data of 1991 Meiyu season over China, we conducted coupled-model experiments, and found that: (i) For the whole model domain, the consideration of the two heterogeneities, in which intrapatch variability plays a very important role, greatly affects the simulations for the surface flux, wind, temperature and precipitation fields. (ii) The temperature and heat fluxes are quite sensitive to the heterogeneities, which displays the following rule: for a sub-region, the mean sensible heat flux decreases, the mean latent heat flux increases, and the mean surface temperature decreases with the increase of the heterogeneities. Furthermore, the mean latent heat flux is more sensitive to the heterogeneities than the mean sensible heat flux. (iii) It seems that the influence of stomatal-resistance heterogeneity on the latent heat flux is greater than that of roughness-length heterogeneity. Therefore, it is necessary to appropriately represent subgrid land-surface heterogeneities so as to improve regional climate modeling.

1. Introduction

The land surface is a key component of the earth's climate system, and is characterized by significant heterogeneities. In the last decade or so, there have been an increasing number of land surface parameterizations considering these heterogeneities (Avissar and Pielke, 1989; Koster and Suarez, 1992; Avissar, 1992; Seth et al, 1994; Li and Avissar, 1994; Leung and Ghan, 1995; 1998; Sivapalan and Woods, 1995; Giorgi, 1997a; Liu et al, 1999; Walko et al, 2000; Wang et al, 2000). As indicated by Giorgi and Avissar (1997), the effects of surface heterogeneity can be grouped in two categories (i.e., ''aggregation'' and ''dynamical'' effects): subgrid scale aggregation has been shown to especially affect the surface latent and sensible heat fluxes, the simulation of snow, and the dynamics of soil moisture and runoff, while dynamical heterogeneity effects are associated with microscale and mesoscale circulations induced by heterogeneous surfaces. The effects of the heterogeneities are such that it is necessary to represent them

in land surface schemes for use in climate models.

Currently, land surface models are all based on ''big leaf'' theory, in which a model grid cell is subdivided into some ''patches'' to consider spatial variability, and in which interpatch variability is mostly taken into account while seldom intrapatch variability. Among different approaches in the land surface model, the mosaic approach has been mostly applied to describe interpatch variability (Avissar and Pielke, 1989; Koster and Suarez, 1992; Leung and Ghan, 1995), while the statistical-dynamical approach, in which heterogeneity is described in terms of probability density functions (PDFs), is used to represent intrapatch variability and can be classified into two types, the numerical type (e.g., Li and Avissar, 1994) and the analytical type (e.g., Entekhabi et al, 1989). Obviously, the combination of the Mosaic approach and the analytical type of statistical-dynamical approach can fully account for the surface heterogeneities and is computationally efficient.

The above efficient method was adopted by Giorgi (1997a). He subdivided a grid cell into fractional areas covered by basic surface types (e.g., vegetated, bare soil, snow-covered surfaces), which separately exchange momentum, energy, and moisture with the atmosphere. Within each surface type, heterogeneity is described by assuming that variables (i.e., surface temperatures and moistures) follow continuous analytical PDFs and by integrating relevant nonlinear terms over the appropriate PDF. Besides, linear and symmetric PDFs are chosen since they allow ready analytical integration and can represent the first-order effects of heterogeneities. Giorgi (1997b) used the model and performed some off-line experiments.

As indicated by Pitman et al (1990), ''advances in land-surface modeling must be made in tandem with improvements in the coupling between the land surface and atmosphere''. In the study considering sub-grid spatial variability by Liang et al (1996), the authors noted that, the feedback effects are not included in their off-line study, and atmospheric feedback effects are potentially important and would be a focus of future study. In facts, the off-line experiments are very limited when accounting for strong, nonlinear interactions between the surface and overlying atmosphere.

The present study is intended to conduct coupled-model simulations to investigate the influences of the land surface heterogeneities on the regional climate with an approach for heterogeneity representation similar as Giorgi (1997a). There are many heterogeneities at the land surface, in this paper, however, we only focus on two primary ones, the heterogeneities in roughness length and stomatal resistance (other than in moisture and temperature as Giorgi, 1997a for the sake of paper length). Then, it's very natural for us to expect that regional climate might display a certain sensitivity to the heterogeneities. Here arise two questions: (1) To what extent do the heterogeneities affect the regional climate? (2) Is there any rule in the modeled regional climate affected by the heterogeneities? If the answers are definitely given, they would be very conductive for the regional climate modeling, that is, we can evaluate regional climate modeling that is performed without inclusion of heterogeneity effects according to what we have investigated with the inclusion.

In Sect. 2, the description of the regional climate models used here is firstly provided, Sect. 3 addresses the results of the sensitivity experiments, and the summary and discussion are presented in Sect. 4.

2. The regional climate model

This section describes the regional climate models and the design of sensitivity experiments. Two models are used here, one is the NCAR (National Center for Atmospheric Research) regional climate model RegCM2 (Giorgi et al, 1993a, b), and the other is based on RegCM2 with heterogeneity representation. That is, the only difference between the two models is that the latter includes heterogeneity treatment.

The land surface scheme employed in RegCM2 is BATS (Dickinson et al, 1993). Since there have been many studies on RegCM2 (e.g., Giorgi et al, 1999), in this section, the focus is the treatment of roughness-length and stomatal-resistance heterogeneities in BATS as well as experimental design.

2.1 Heterogeneity treatment

In this paper, roughness-length heterogeneity and stomatal-resistance heterogeneity are treated,

respectively. Following is the brief descriptions of the treatment.

Roughness length affects surface fluxes, and is directly associated with drag coefficient. In BATS, the representative value of drag coefficient is a weighted average over different types of land surface at the grid cell. For a given land type, C_{DN}, the drag coefficient under neutral condition, is the function of roughness length (z_0) and the height of the lowest atmospheric-model level (z_1):

$$C_{DN} = \left[\frac{k}{\ln[(z_1 - d_0)/z_0]}\right]^2, \tag{1}$$

where k is von Karman constant, z_1 varies little in a given atmospheric model, and d_0, the zero plane displacement height, is introduced when obstacles (e.g., buildings, trees and even crops) exist. As a general treatment, z_0 can be regarded as a fraction of the height of the obstacle (e.g., $1/10$), d_0 also a fraction (e.g., $8/10$), then d_0 is a multiple of z_0 (i.e., $d_0 = d_{00} \times z_0$, where d_{00} is a constant). So, the heterogeneity of d_0 is taken into account as long as that of z_0 is, and C_{DN} can be assumed to change only with z_0. In the cases without obstacles (e.g., bare soil, sea surface), $d_0 = 0$ is taken. Therefore, we obtain

$$C_{DN} = \left[\frac{k}{\ln(z_1/z_0 - d_{00})}\right]^2. \tag{2}$$

The above equation demonstrates that a distribution of z_0 corresponds to a determined distribution of C_{DN}, and vice versa. Rather than assuming the independent variable of PDFs to be fundamental variables, e.g., soil moisture (e.g., Entekhabi et al, 1989; Giorgi, 1997a), we assume the independent variable to be the functions of fundamental variables, which is more universal and feasible. For simplicity, here we assume

$$y = \ln[(z_1 - d_0)/z_0], \tag{3}$$

and employ $f_{pdf}(y)$ as a linear and symmetric PDF (Giorgi, 1997a), therefore y is the independent variable of $f_{pdf}(y)$, the function. Assume the average, half width and height ratio of y denoted by y_0, α, γ, respectively, and introduce heterogeneity operator (Giorgi, 1997a),

$$F^x_{pdf}(A) = \int A f_{pdf}(x)dx, \tag{4}$$

where A is a term nonlinear with respect to x, the heterogeneous variable, then the average of A is represented by the above equation. Similarly, as y and $f_{pdf}(y)$ are introduced, the heterogeneity treatment of C_{DN} is obtained:

$$F^y_{pdf}(C_{DN}) = \int C_{DN} f_{pdf}(y)dy, \tag{5}$$

which allows analytical integration over the whole distribution.

Similarly, the average expression of z_0 after heterogeneity treatment is obtained by

$$\begin{aligned} F^y_{pdf}(z_0) &= \int z_0 f_{pdf}(y)dy \\ &= \int z_0 f_{pdf}[y(z_0)](dy/dz_0)dz_0. \end{aligned} \tag{6}$$

Since C_{DN} is a single valued function of z_0, in terms of mathematics, it is necessary to deal with other characteristics or terms associated with z_0 or C_{DN} (e.g., Snow coverage f_{SNOW} The wind speed within the foliage layer U_{af}, aerodynamical resistance at the foliage layer r_{la}). Besides, the heterogeneity in stomatal resistance is also included in this study. For details, see Appendix.

2.2 Experimental design

On the basis of the above subsection, a new regional climate model, here referred as RCM1 with a corresponding new land surface scheme (BAT1), is constructed. For simplicity, the standard version of RegCM2 is hereafter referred to as RCM0 corresponding to BATS (Dickinson et al, 1993, hereafter referred to as BAT0). Hence RCM0 (BAT0) is different from RCM1 (BAT1) only in whether the heterogeneities are considered or not. By use of different models with different extents of the heterogeneities, the sensitivities of the model-produced climate can be analyzed.

2.2.1 Design of model mesh

The model domain covers the area within 24.7–45.7° N and 100.88–133.12° E. The center of the simulated domain is located at 35.20° N/117.00° E. The grid resolution is 60 km with the grid number 41×40. Vertical levels of the model are set nonuniformly with 11 integral levels (i.e., $\sigma = 0.0$, 0.15, 0.30, 0.45, 0.60, 0.75, 0.85, 0.93, 0.97, 0.99, 1.00) and 10 half levels (for mostly output), which are located between 11 integral levels.

2.2.2 Option of model physics and dataset

Both models apply the same model physics, e.g., Holtslag's planetary boundary-layer scheme (Holtslag et al, 1990; Holtslag et al, 1993), time-dependent, exponentially nudging lateral boundary scheme, the modified Kuo-type cumulus parameterization scheme (Anthes et al, 1987), etc., and the same dataset, i.e., 3-month observational data during 1991 Meiyu season (May–July) when a catastrophic flood occurred, are used so as to confirm the comparability of the experiments. The only difference among the simulations lies in the extent of heterogeneity (see Table 3).

2.2.3 Choice of PDF parameters

When the PDF and its independent variable are chosen, it is necessary to choose suitable PDF parameters (i.e., half width α and height ratio γ) so as to represent the first-order heterogeneity.

Apparently, the greater α, the wider the range of the PDF independent variable; the closer to 1 the value of γ, the more heterogeneous the PDF independent variable distributed over the same range. As for performing simulations, we suggest, it must be followed that the chosen PDF parameters should be relatively consistent with the used model and the properties of the simulated domain.

As an example, some results of Exp.1 computed according to the PDF of z_0 (see Appendix) are given in Table 1. From the table, we can see that, the heterogeneity in y can result in a large change in the averaged values of drag coefficient and snow cover. Besides, with low y heterogeneity (denoted by small values of α_n, e.g., 0.001), the treated-characteristic values are close to those without heterogeneity treatment, which confirms the expressions for treatments mentioned above and can be proved with rigorous mathematical method.

Furthermore, $h_{pdf}(z_0)$, the PDF of z_0, still displays a single-peak pattern, just like what $f_{pdf}(y)$ illustrates (see Fig. A.1 in Appendix).

Shown in Table 1, α_n has an upper limit which is generally smaller than about 0.6. Because the value of the chosen γ does not lead to physical mistakes (e.g., the value of the heterogeneous characteristic exceeds the reasonable range), here we only discuss the choice of width ratios corresponding to y and to stomatal resistance r_s, when performing simulations with RCM1.

Table 2 shows the experiment results of PDF parameters chosen in RCM1, where α_n, γ, z_{00}, z_1 and d_{00} are the inputs, the others are output results; C_{DN0} and z_{00} are drag coefficient and roughness length without heterogeneity treatment; C_{DN1} and z_{01} which are appended with subscript "1" denote drag coefficient and roughness length with heterogeneity treatment, respectively; r_{cdn} and r_{z_0} are the ratios of drag coefficient and roughness length with heterogeneity to their corresponding values; $z_{0\,\min}$ and $z_{0\,\max}$ are the lower and upper limits of z_0 after heterogeneity treatment, respectively.

From Table 2, it can be seen that the average of roughness length will be increased after heterogeneity treatment (i.e., $r_{z_0} > 1$). Since values of z_{00}, z_1 and d_{00} are close to those inputs in BAT0 in the case of vegetation, under the assumption of roughness length z_0, which was classified by Olson et al (1983), to be a specific average (even though it is very approximate), in order to approximate z_{01} (a value for z_0 after heterogeneity treatment) to z_0 given by classification, the ratio c_{00} of

Table 1. Results of heterogeneity treatment in Exp.1 ($z_1 = 40$ m, $z_{00} = 2.69 \times 10^{-2}$ m, $Sr = 0.01$ m, $\gamma = 0.8$). r_{cdn}, r_{fsn}, r_{uaf}, r_{rai} and r_{z_0} are the ratios of drag coefficient (C_{DN1}), snow cover, within-foliage wind, transfer coefficient at foliage layer, and roughness length (z_{01}) with heterogeneity treatment to the corresponding characteristics without heterogeneity treatment. $z_{0\,\min}$ and $z_{0\,\max}$ are the minimum and maximum values of roughness length z_0, z_{00} is the average of z_0. For simplicity, here α, an input parameter, is replaced by α_n, width ratio that is defined as the ratio of α to the average of y, or to the PDF independent variable without heterogeneity treatment

	$z_{0\,\min}$ ($\times 10^{-2}$ m)	$z_{0\,\max}$ ($\times 10^{-2}$ m)	z_{01} ($\times 10^{-2}$ m)	C_{DN1} ($\times 10^{-3}$)	r_{cdn}	r_{fsn}	r_{uaf}	r_{rai}	r_{z_0}
$\alpha_n = 0.001$	2.67	2.71	2.70	2.999	0.99998	0.99960	0.99998	0.99998	0.99999
$\alpha_n = 0.1$	1.30	5.59	2.92	3.029	1.0095	1.0265	1.0032	1.0012	1.0862
$\alpha_n = 0.3$	0.301	24.1	5.27	3.28	1.0932	1.1872	1.0299	1.0111	1.9548
$\alpha_n = 0.6$	0.0337	215	23.0	4.58	1.5266	1.4210	1.1459	1.0509	8.5625

Table 2. Experiments for PDF parameter choice. PDF here directly corresponds to y, the single valued function of z_0, with $z_1 = 38.4$ m and $d_{00} = 9$ (the ratio of zero plane displacement to z_0, see text). The other symbols are the same as Table 1

No.	α_n	γ	z_{00} (m)	$z_{0\,\min}$ (m)	$z_{0\,\max}$ (m)	z_{01} (m)	r_{z_0}
1	0.2	0.001	1.00	5.75×10^{-1}	1.60	1.34	1.34
2	0.4	0.001	1.00	3.13×10^{-1}	2.31	1.47	1.47
3	0.6	0.001	1.00	1.65×10^{-1}	2.98	1.63	1.63
4	0.2	0.9	1.00	5.75×10^{-1}	1.60	1.05	1.05
5	0.4	0.9	1.00	3.13×10^{-1}	2.31	1.13	1.13
6	0.6	0.9	1.00	1.65×10^{-1}	2.98	1.25	1.25
7	0.2	0.001	0.80	4.26×10^{-1}	1.38	0.98	1.23
8	0.4	0.001	0.71	1.79×10^{-1}	2.04	0.98	1.38
9	0.6	0.001	0.58	5.92×10^{-2}	2.74	0.99	1.71
10	0.2	0.9	0.95	5.38×10^{-1}	1.55	1.00	1.05
11	0.4	0.9	0.84	2.34×10^{-1}	2.17	0.98	1.17
12	0.6	0.9	0.76	9.55×10^{-2}	2.85	1.04	1.37

Table 3. PDF parameters chosen in the experiments, in which α_n and γ represent width ratio and height ratio, respectively, both are in form of the function of y or r_s; d_{00} and c_{00} are inputs associated with the roughness length

	EPT00	EPT01	EPT02	EPT03	EPT04	EPT05	EPT06	EPT07	EPT08	EPT09	EPT10	EPT11	EPT12
$\alpha_n(y)$	–	0.1	0.3	0.5	0.1	0.3	0.5	0.5	0.5	0.5	0.5	0.5	0.5
$\gamma(y)$	–	0.9	0.9	0.9	0.9	0.9	0.9	0.4	0.1	0.9	0.9	0.9	0.9
$\alpha_n(r_s)$	–	0.3	0.3	0.3	0.3	0.3	0.3	0.3	0.3	0.3	0.5	0.7	0.5
$\gamma(r_s)$	–	0.06	0.06	0.06	0.06	0.06	0.06	0.06	0.06	0.06	0.06	0.06	0.8
d_{00}	–	9	9	9	9	9	9	9	9	9	9	9	9
c_{00}	–	0.7	0.7	0.7	0.9	0.9	0.9	0.7	0.7	0.7	0.7	0.7	0.7

the input z_{00} to z_0 must be within the range from 0.6 to 0.95. Based on all these, the heterogeneity is considered. For example, in the 9th row of Table 2, $z_{01} = 0.99$ m, which is close to the classification ($z_0 = 1$ m), when $z_{00} = 0.58$ m. So for the original classification $z_0 = 1$ m, we input $z_{00} = 0.58$ m. On the basis of this we change z_0 in BAT0 to the other value in BAT1, and then use the changed value to calculate the treated values of the expressions of relevant characteristic quantities (e.g., drag coefficient, snow coverage, etc.).

The heterogeneity in stomatal resistance r_s is also considered in RCM1. Since many factors affecting r_s are very complicated, the spatial distribution of r_s is highly heterogeneous, there are a lot of controversies about r_s treatments in the land surface models (Carlson, 1991), most of the r_s equations are given empirically (Avissar, 1993), and the minimum r_s in BAT0 produced too low evaporation and too high sensible heat flux compared to observations (Giorgi, 1997b). Therefore, in this paper, the output value of the BAT0 algorithm is used as the average in the distribution, and the width ratio of r_s to be smaller than or equal to 0.30.

All the parameters in the experiments (EPT00–EPT12) are given in Table 3, where $\alpha_n(y)$ and $\gamma(y)$ respectively denote the width ratio (ratio of half width to the average) and height ratio of y; $\alpha_n(r_s)$ and $\gamma(r_s)$ correspond to those for the stomatal resistance, respectively; d_{00} is the ratio of zero plane displacement to the roughness length, and c_{00} represents the ratio of the input roughness length to the roughness length given by the classification in BAT0. Among the experiments, EPT00 employs RCM0 while others applying RCM1.

3. Model results due to heterogeneities

In the analysis of model results, we focus on the simulated 3-month-mean fields for the domain. Meanwhile, due to the different features of temperatures and moistures over the southern and northern parts of China, we also pay great attention to the JHR region, which represents part of the southern China and is characterized by its warm and humid climate, and to the HBR region, which represents part of the northern China and is characterized by its relatively cool and arid

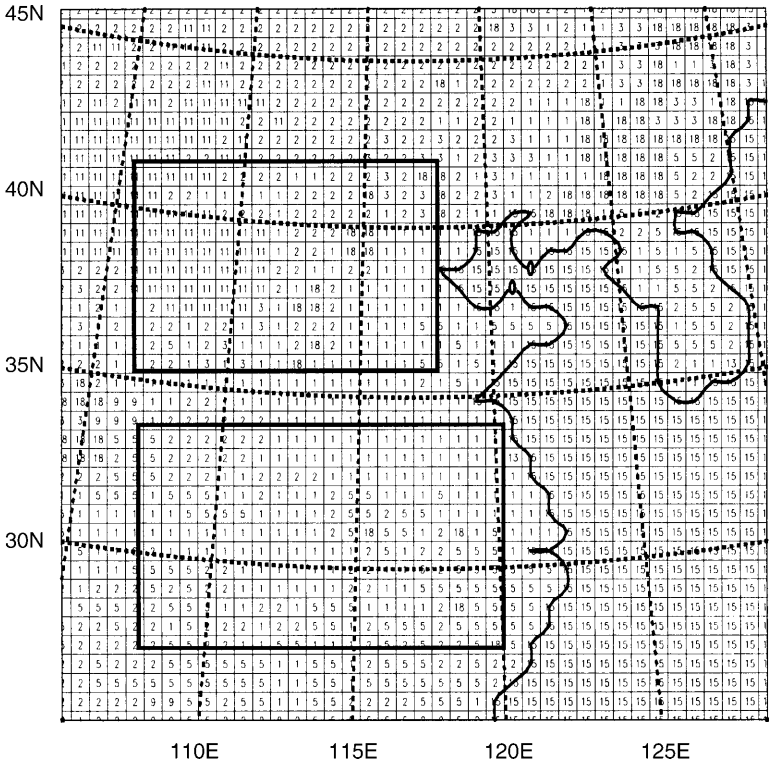

Fig. 1. Model domain and investigated regions, where the upper and lower rectangles denote the HBR and JHR regions, respectively; and land cover types are set according to BATS (1, crop; 2, short grass; 3, evergreen needleleaf tree; 4, deciduous needleleaf tree; 5, deciduous broadleaf tree; 6, evergreen broadleaf tree; 7, tall grass; 8, desert; 10, irrigated crop; 11, semi-desert; 15, ocean; 18, mixed woodland)

climate. Both regions are shown in Fig. 1. The 13 experiments are analyzed according to the features of the heterogeneities, i.e., the PDF width ratios and height ratios.

In addition to 3-month-mean quantities, the differences between the experiments are stressed on so as to show the sensitivities of the simulated climate to the heterogeneities. For example, the major differences in temperatures are *D*tgm (the maximum of absolute differences between the values of $Tg(i,j)$, the 3-month-mean surface temperature at a grid cell (i,j) for the relevant experiment, and that for EPT00), and *A*dtg (the regional-average absolute difference between $Tg(i,j)$ and that for EPT00). That is, *D*tgm is calculated by

$$D\text{tgm} = \max|[Tg(i,j) - Tg_{00}(i,j)]|, \tag{7}$$

where $Tg_{00}(i,j)$ corresponds to $Tg(i,j)$ but for EPT00; and *A*dtg is obtained by

$$A\text{dtg} = \frac{1}{N}\sum_{i,j}|[Tg(i,j) - Tg_{00}(i,j)]|, \tag{8}$$

where N is the number of the grid points in the given region. Apparently, the larger *D*tgm and *A*dtg, the more significant heterogeneity. *T8*, *D*t8m and *A*dt8 are quantities for 850 hPa air temperature, while *Sh*, *D*shm and *Ad*sh for surface sensible heat flux, and *Lh*, *D*lhm and *Ad*lh for surface latent heat flux, which correspond to *Tg*, *D*tgm and *A*dtg, respectively. All these results are listed in Table 4.

Besides, two kinds of characteristic differences $Q_{\rm gm}$ and $Q_{\rm r}$ ("Q" represents a quantity, e.g., $Tg_{\rm gm}$ and $Tg_{\rm r}$ for the surface temperature, $SH_{\rm gm}$ and $SH_{\rm r}$ for the sensible heat flux, while $LH_{\rm gm}$ and $LH_{\rm r}$ for the latent heat flux.), whose algorithms are similar to *D*tgm and *A*dtg but for two relevant tests (e.g., EPT01 and EPT02), are statistical quantities used in the following analyses (not given in Table 4).

In this section, the sensitivities to roughness-length and stomatal-resistance heterogeneities are analyzed in the following, respectively.

3.1 Sensitivities to roughness-length heterogeneity

Firstly in this sub-section, we analyze the results of sensitivity tests for roughness-length heterogeneity according to different PDF parameters.

3.1.1 Experiments with respect to width ratio

In order to explore the sensitivities of the regional climate to width ratios, 3 experiments, i.e.,

Table 4. Some results of the experiments. All values are for 3-month-mean quantities. That is, *Tg*, *D*tgm and *A*dtg represent respectively the regionally-averaged surface temperature, the maximum absolute difference in surface temperature for grid points between relevant experiment and EPT00, and the mean absolute the difference; *T8*, *D*t8m and *A*dt8, *Sh*, *D*shm and *Ad*sh, and *Lh*, *D*lhm and *Ad*lh all correspond to *Tg*, *D*tgm and *A*dtg, but for the 850 hPa temperature, and the surface sensible and latent heat fluxes, respectively. Apart from *Ps*, which represents the maximum precipitation amount for June in JHR region and corresponds to an observed value of 478 mm, the upper-row value of the two for a quantity in an experiment is for the JHR region, while the lower-row value for the HBR region

	EPT00	EPT01	EPT02	EPT03	EPT04	EPT05	EPT06	EPT07	EPT08	EPT09	EPT10	EPT11	EPT12
Tg[K]	300.17	300.15	300.14	300.04	300.17	300.21	300.14	300.05	300.17	300.04	300.12	300.14	300.10
	297.50	297.26	297.02	296.99	297.26	297.16	296.91	296.79	297.08	296.99	296.97	297.10	296.88
*D*tgm[K]	–	1.58	1.19	1.25	1.62	1.48	1.79	2.05	1.49	1.25	2.05	1.30	1.28
	–	1.83	2.44	2.38	2.07	1.95	2.81	2.47	2.02	2.33	2.13	2.37	2.24
*A*dtg[K]	–	0.31	0.31	0.30	0.28	0.33	0.32	0.33	0.30	0.30	0.37	0.28	0.33
	–	0.55	0.62	0.66	0.57	0.54	0.80	0.75	0.60	0.66	0.74	0.61	0.72
T8[K]	292.41	292.38	292.40	292.43	292.50	292.44	292.46	292.45	292.48	292.47	292.48	292.47	292.45
	291.02	290.99	290.88	290.93	291.00	290.94	290.99	290.86	290.97	290.93	291.01	291.03	290.87
*D*t8m[K]	–	0.13	0.19	0.18	0.11	0.15	0.25	0.18	0.20	0.18	0.25	0.24	0.17
	–	0.22	0.30	0.27	0.15	0.30	0.35	0.36	0.27	0.27	0.23	0.27	0.30
*A*dt8[K]	–	0.04	0.05	0.07	0.03	0.04	0.10	0.05	0.06	0.07	0.07	0.06	0.06
	–	0.06	0.15	0.12	0.07	0.09	0.10	0.17	0.08	0.12	0.08	0.09	0.16
Sh[W/m^2]	7.04	6.92	6.36	4.71	6.73	6.28	5.38	4.91	5.73	4.71	4.56	3.40	3.99
	22.84	22.29	19.68	18.59	20.69	20.22	19.06	17.93	19.39	18.59	17.84	18.25	17.52
*D*shm[W/m^2]	–	12.5	12.7	12.6	9.1	11.8	23.9	16.8	14.6	12.6	14.8	18.6	15.2
	–	13.6	22.3	23.5	18.7	19.1	26.3	26.2	21.0	23.5	27.7	24.0	27.1
*Ad*sh[W/m^2]	–	2.73	2.44	3.05	2.30	2.60	3.34	3.16	2.85	3.05	3.63	4.11	3.64
	–	4.87	5.78	6.08	5.84	5.19	7.29	6.14	5.67	6.08	6.94	6.75	7.06
Lh[W/m^2]	91.4	91.2	92.4	95.6	91.5	92.2	94.4	94.5	93.8	95.6	95.4	97.3	96.6
	98.07	98.95	99.07	102.69	98.49	98.99	102.83	101.87	100.77	102.69	103.19	103.84	104.58
*D*lhm[W/m^2]	–	15.8	15.9	17.7	17.2	12.8	13.0	12.3	12.5	17.7	15.5	22.3	18.8
	–	19.5	32.7	31.1	21.5	22.8	26.4	27.7	22.0	31.2	28.1	31.7	28.7
*Ad*lh[W/m^2]	–	3.21	3.43	4.92	2.64	3.31	4.42	4.36	3.74	4.92	4.81	6.23	5.65
	–	6.31	5.87	6.97	5.87	5.36	8.12	7.01	6.13	6.97	7.45	7.74	8.32
Ps[mm]	615	758	594	548	763	579	572	698	476	548	627	646	497

EPT01, EPT02 and EPT03 corresponding to $\alpha_n(y) = 0.1$, 0.3 and 0.5, respectively, are designed different from each other only in width ratios. As shown in Table 1, a larger $\alpha_n(y)$ corresponds to a larger C_{DN}, the drag coefficient under neutral condition, that is, the more heterogeneous roughness-length distribution, the stronger turbulent transportation under neutral condition. Therefore, a larger C_{DN} corresponds to larger absolute values in turbulent fluxes under the same boundary-layer forcings. However, the relation between $\alpha_n(y)$ and surface fluxes should be more complex in coupled-model simulations due to many factors, e.g., the constant energy inputs to the model domain and complex nonlinear interactions between the surface and the atmosphere. Firstly we discuss the simulation for the JHR region. From the results, the maximum sensible heat flux difference SH_{gm} between EPT01 and EPT03 can be up to 19.2 W/m^2 at a grid point, the mean difference SH_{r} reaches 3.24 W/m^2. Compared with the mean sensible heat flux *Sh* of about 6 W/m^2 over the region, the spatial variability of sensible heat fluxes among different grid points affected by the heterogeneity is quite large. Correspondingly, the maximum latent heat flux difference LH_{gm} between EPT01 and EPT03 can be up to 21.4 W/m^2, the mean difference LH_{r} reaches 5.06 W/m^2. We suggest that these values are quite large, as compared to the Earth's surface flux balance of CO_2 doubling which would reduce the thermal radiation flux by about 4 W/m^2 (Houlton, 1997). The simulated surface temperature difference Tg_{gm} can reach 1.84 K,

with the mean difference Tg_r of 0.37 K. And the mean deviation of 0.37 K of surface temperature are also quite large, as compared to the increase of about 0.5 K of the global warming during the last century or so (Houlton, 1997). All this shows that, the temperature fields are sensitive to the heterogeneity due to roughness-length distribution range, and the local/grid-point difference is very large. From the comparison of the differences between EPT01 and EPT03 and corresponding differences between EPT01 and EPT02, a greater sensitivity caused by larger $\alpha_n(y)$ can be seen (Table 4). Besides, the values of *Ps*, the maximum precipitation amount for June, are 758 mm, 594 mm and 548 mm in EPT01, EPT02 and EPT03 (Table 4), respectively, which displays a great difference, and in which EPT03 with the largest roughness-length heterogeneity can well reflect the observed maximum of 478 mm, implying that appropriate representation of roughness-length heterogeneity can improve the simulations for precipitation.

Analogous results can be found in the simulation for the HBR region. In Table 4, we can see that the temperature fields are very sensitive to roughness-length heterogeneity, and the heat fluxes are quite sensitive. In addition, these sensitivities display a rule (or a feature): for a certain region, with the increase (decrease) of roughness-length heterogeneity, i.e., with the increase (decrease) of $\alpha_n(y)$, the mean sensible heat flux *Sh* decreases (increases), the mean latent heat flux *Lh* increases (decreases), and the mean surface temperature *Tg* decreases (increases). Because the changes of both the mean heat fluxes are just a partition of energy for the region with each has an opposite sign to the other, and when the change of the mean latent heat flux is greater than that of the mean sensible heat flux (this is generally the case for a humid region, as discussed later in this subsection), the surface temperature should changes correspondingly in such a way that the radiative-flux change could add to the approximate balance of the fluxes. Consequently, the above rule shows itself. As for the mean surface temperature (the mean 850 hPa temperature and surface sensible heat flux as well), the variation in the HBR region is larger than that in the JHR region. Thus, we can see, the influence extent of roughness-length heterogeneity differs from region to region due to various conditions of vegetation, e.g., vegetation types, coverages and growth phases.

In Table 4, *Ad*sh, the absolute difference in 3-month mean surface sensible heat fluxes compared to EPT00, can amount to about $3\,W/m^2$ ($6\,W/m^2$) for the JHR (HBR) region in the 3 experiments; similar is *Ad*lh, the absolute difference in 3-month mean surface latent heat fluxes. Generally, the values of *Ad*lh are greater than those of *Ad*sh in both regions, as can be seen in other experiments. This shows that the latent heat flux is more sensitive to the heterogeneities than to the sensible heat flux. By conducting off-line experiments with a land surface scheme (PLAID), Li and Avissar (1994) indicated that the latent heat flux was the most sensitive to spatial variability compared to the sensible heat and radiative fluxes. We further confirm part of this conclusion by performing coupled-model simulations with a different land surface scheme (BAT1).

The simulation of the whole domain is similar to those for partial regions in the domain, as can also be seen from Table 4. It should be noted that, although the previous sub-section reveals that the mean sensible heat flux is less sensitive to the heterogeneity than the mean latent heat flux for a region, the mean sensible heat flux may be more sensitive than the mean latent heat flux for a grid cell.

Figure 2 presents a comparison of the simulations of EPT01 and EPT03. From the systematic fields at 850 hPa (Fig. 2b), the temperature over most part of the southern domain in EPT03 is higher than that in EPT01, while the temperature over most part of the northern domain in EPT03 is lower than that in EPT01. Correspondingly at the surface, the temperature is lower by over 0.5 K over a large area in EPT03 compared to EPT01, while there is a slightly warmer area in the south (Fig. 2a) in EPT03. The patterns of temperature changes are consistent with those of the sensible and latent heat fluxes illustrated in Fig. 2c, d.

During the Meiyu season in 1991, most of the rainfall occurred in June. Figure 3a–c illustrate the June precipitation amounts of observations and simulations. From Fig. 3b and c, due to the same lateral boundary forcing, the precipitation patterns are similar, however, owing to the effects of heterogeneity, great difference between

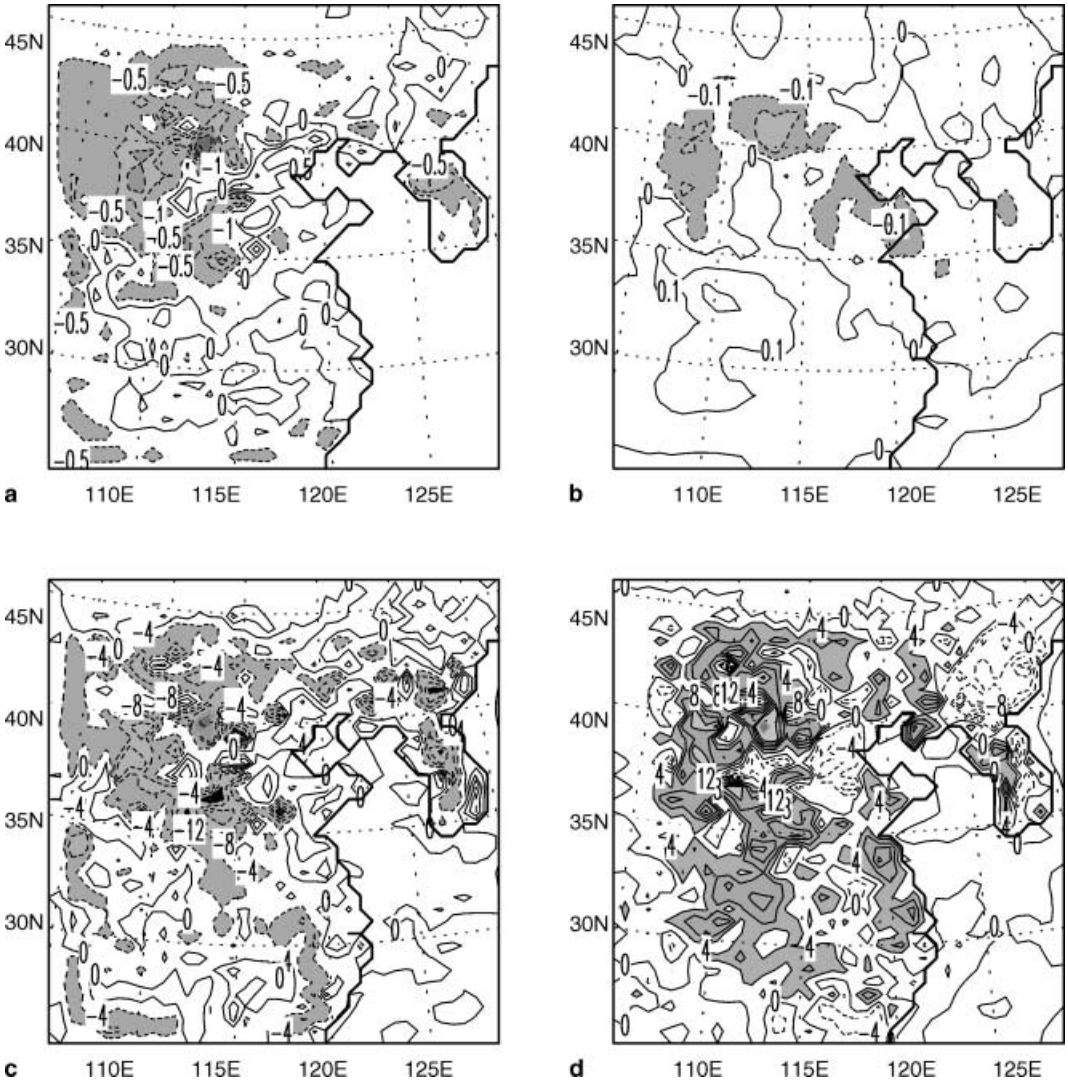

Fig. 2. Comparison of EPT01 and EPT03, where differences of the ground surface and 850 hPa air temperatures, and the sensible and latent heat fluxes between EPT03 and EPT01 are plotted in Fig. 2a–d, with contour intervals of 0.5 K, 0.1 K, $4\,W/m^2$ and $4\,W/m^2$, respectively; in Fig. 2a–d, areas with differences smaller than -0.5 K, -0.1 K, $-4\,W/m^2$ and greater than $4\,W/m^2$ are shaded, respectively

the precipitation amounts at the rainbelt centers in EPT01 and EPT03 can still be identified. The rainbelt center in EXP01 is much stronger.

Results from EPT04–EPT06 are similar to those from EPT01–EPT03, which is shown in Table 4.

From all these, it is obvious that the influences of roughness-length heterogeneity on the regional climate modeling of regional surface fluxes, and the flow, temperature and precipitation fields are generally very large. Since both interpatch and intrapatch variabilities are included, and interpatch variability are initially considered as the same in each experiment, all these also show great sensitivities of precipitation, temperature and surface fluxes to intra-patch variability.

3.1.2 Experiments with respect to height ratio

EPT06, EPT07 and EPT08 are different from each other only in height ratios, with $\gamma(y) = 0.9$, 0.4 and 0.1, respectively, and the differences also reflect effects of roughness-length heterogeneity. In the simulation for the JHR region, the difference in SH_{gm} (SH_r) between EPT06 and EPT08 can be up to $30.2\,W/m^2$ ($2.90\,W/m^2$). Similar are the results of other quantities, e.g., LH_{gm}, LH_r and Tg_{gm}. These show that the flux,

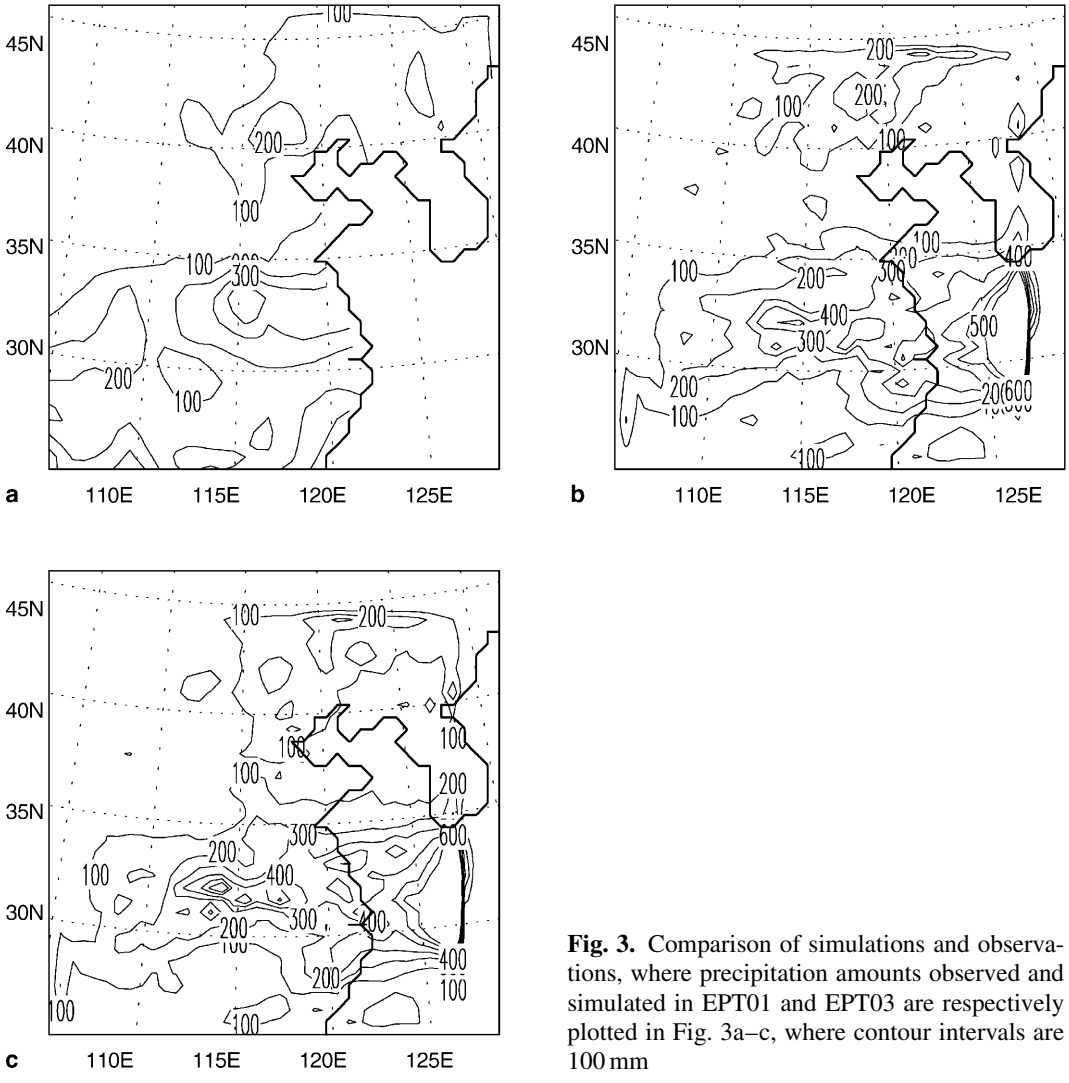

Fig. 3. Comparison of simulations and observations, where precipitation amounts observed and simulated in EPT01 and EPT03 are respectively plotted in Fig. 3a–c, where contour intervals are 100 mm

temperature and precipitation fields are also sensitive to the heterogeneity due to the concentration of roughness-length distributions, as is confirmed by the results in Table 4.

Similar results can be found when we again turn to the simulation for the HBR region (Table 4). We can also identify that the model climate in the HBR region is generally more sensitive than that in the JHR region. For example, for the JHR (HBR) region, the values of the mean surface temperature *Tg* are 300.14 K and 300.17 K (296.91 K and 297.08 K) in EPT06 and EPT08, respectively.

Figure 4 illustrates the comparison of EPT06 and EPT08. As is shown in the 850 hPa-temperature-field difference in EPT08 (Fig. 4b), in contrast to EPT06, the main warmer area lies in the north of the domain, with the increase center over 0.2 K, while the main cooler area lies in the south. Besides, the temperature fields, the surface fluxes and the precipitation field are quite sensitive to the heterogeneity represented by $\gamma(y)$.

3.2 Sensitivities to stomatal-resistance heterogeneity

The results of sensitivity tests for stomatal-resistance heterogeneity are then analyzed according to different PDF parameters in this subsection.

3.2.1 Experiments with respect to width ratio

The stomatal resistance r_s is affected by many factors, e.g., radiation, vapor pressure and soil moisture, which further lead to the heterogeneity. Here EPT09, EPT10 and EPT11, with

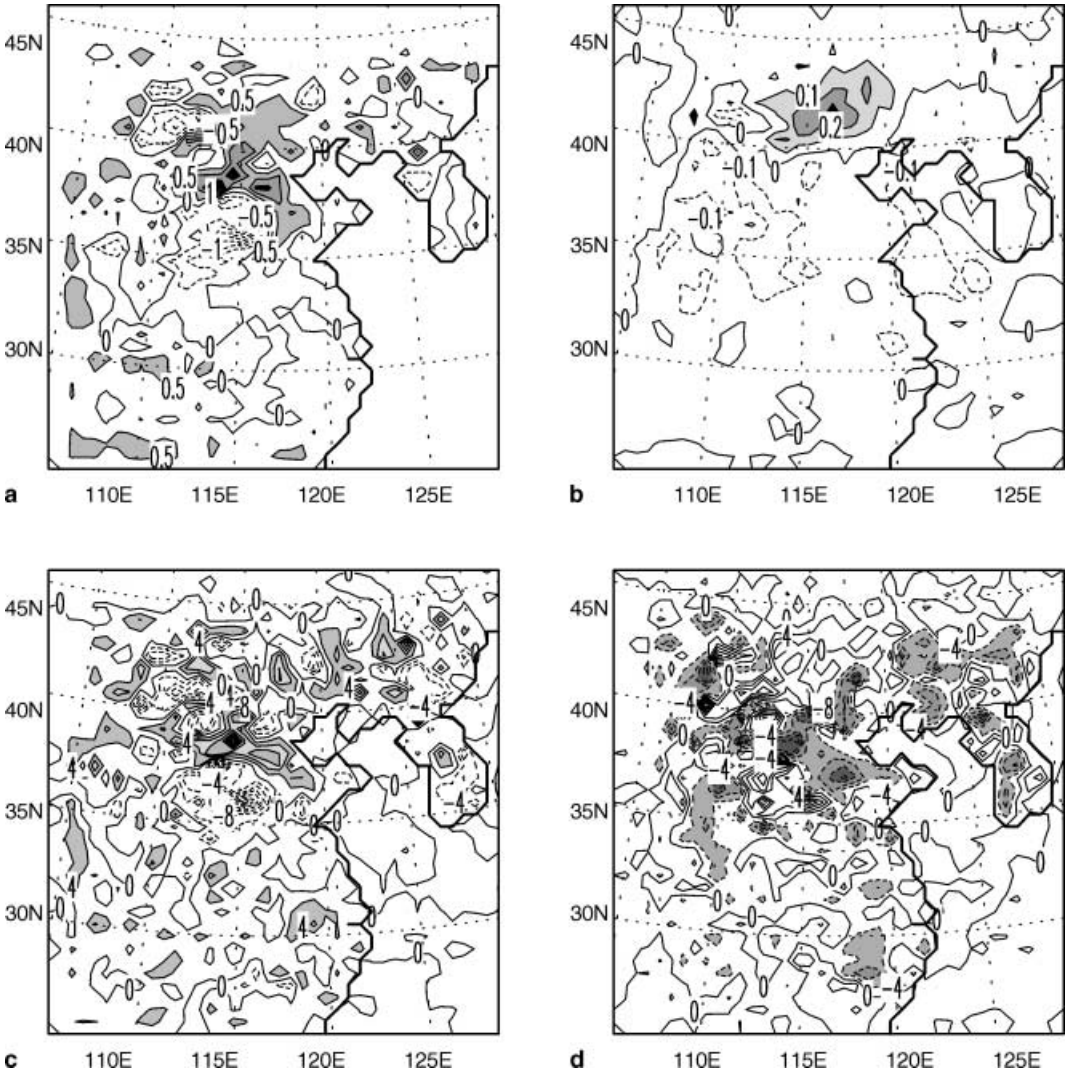

Fig. 4. Comparison of EPT06 and EPT08, where panels are similar to those in Fig. 2, but for differences between EPT08 and EPT06

$\alpha_n(r_s) = 0.3$, 0.5 and 0.7 respectively, are designed in such a way that the sensitivity of the modeled regional climate to stomatal-resistance heterogeneity can be obtained. The 3 experiments are different from each other only in width ratios of r_s. It can be proved via Eq. (A.10) that the more heterogeneous r_s, the larger transpiration rate under a given condition. But the case would be much more complex in the coupled-model simulations due to the changed conditions, e.g., larger transpiration rate might reduce the incoming solar radiation to the leaves, and this might further increase the average of r_s, which reduces transpiration in its turn.

Again, we discuss the simulation for the JHR region firstly. From the results, the difference in SH_{gm} (LH_{r}) between EPT09 and EPT11 can be up to $12.9\,\mathrm{W/m^2}$ ($3.5\,\mathrm{W/m^2}$); the temperature difference in Tg_{gm} (Tg_{r}) amounts to 1.39 K (0.25 K). As presented in Table 4, the mean surface temperature difference between EPT09 and EPT11 reaches 0.1 K; the values of *Ps* in EPT09 and EPT11 are 548 mm and 646 mm, respectively. All these show that the surface fluxes, temperature and precipitation fields are quite sensitive to the heterogeneity due to the distributed range of roughness lengths.

And then we move to the HBR region. Analogous to those in the JHR region, the sensitivities of the heat fluxes to the heterogeneity due to the concentration of stomatal resistance distributions are shown as the similar rule: generally for a certain region, with the increase (decrease) of stomatal-resistance heterogeneity, i.e., with

the increase (decrease) of $\alpha_n(r_s)$, the mean sensible heat flux decreases (increases), and the mean latent heat flux increases (decreases). Furthermore, the influence on the mean latent heat flux due to stomatal-resistance heterogeneity is greater than that due to roughness-length heterogeneity, e.g., in the 13 experiments carried out, it is the experiments (i.e., EPT09, EPT10, EPT11 and EPT12) with relatively large stomatal-resistance heterogeneity that have the relatively large mean latent heat fluxes and relatively small mean sensible heat fluxes.

The analysis for the two regions is consistent with that for the whole domain. Figure 5 illustrates the comparison of EPT09 and EPT11. From the 850 hPa temperature field in EPT11, in contrast to EPT09, there is a large warmer area in the simulated domain with an increase over 0.1 K. Besides, the temperature fields, the surface fluxes and the precipitation field are quite sensitive to the heterogeneity due to different ranges of stomatal-resistance distributions.

3.2.2 Experiments with respect to height ratio

Here we design EPT10 and EPT12, which are different from each other only in height ratios of r_s and correspond to $\gamma(r_s) = 0.06$ and 0.8, respectively, so as to test the sensitivity of the modeled regional climate to stomatal-resistance heterogeneity.

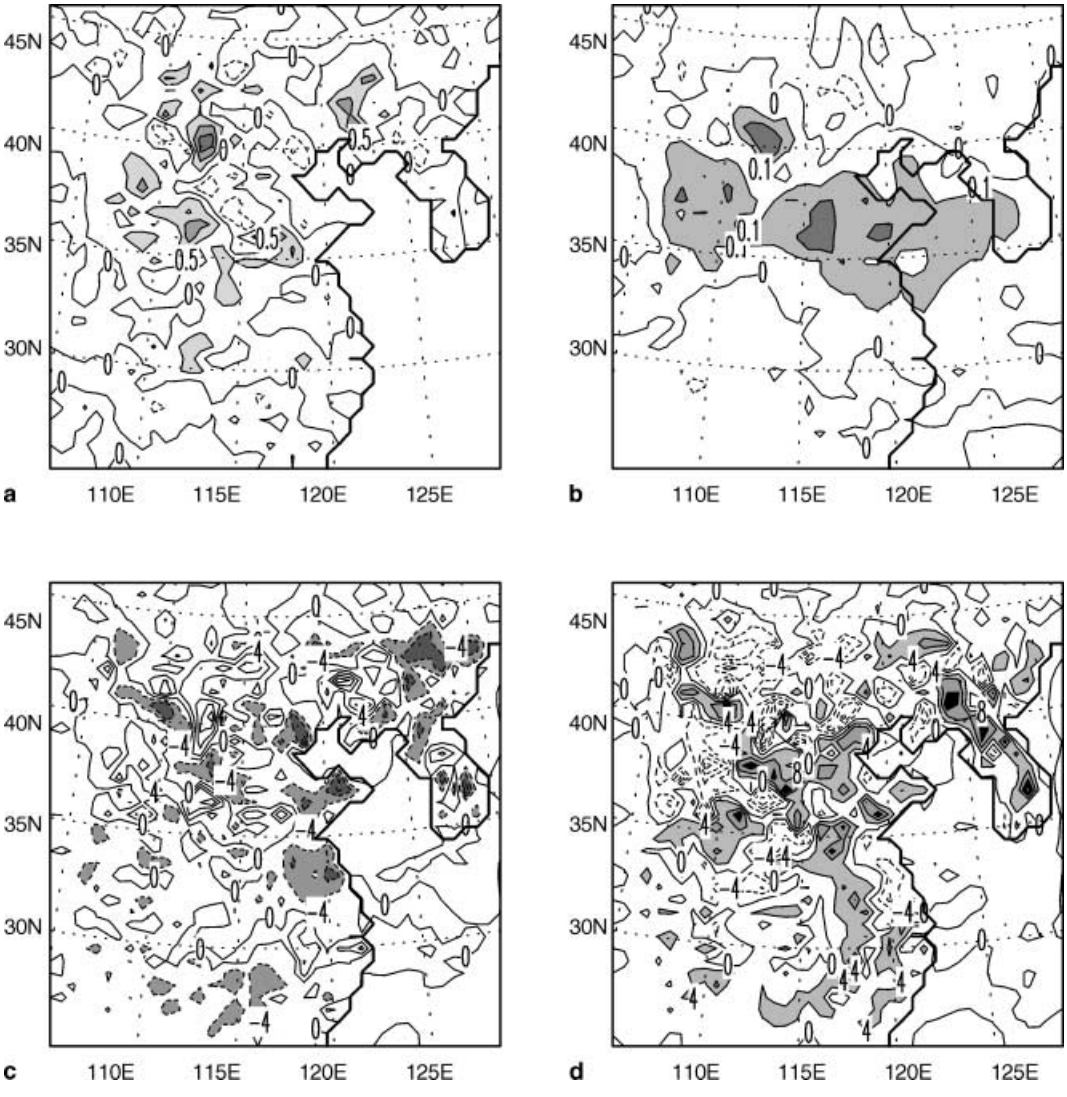

Fig. 5. Comparison of EPT09 and EPT11, where panels are similar to those in Fig. 2, but for differences between EPT11 and EPT09

Again, we start with the discussion of the JHR region in the simulations. From the results, the differences between EPT10 and EPT12 seem to be quite large, e.g., the value of SH_{gm} (SH_r) reaches 10.5 W/m^2 (2.66 W/m^2); correspondingly, the value of LH_{gm} (LH_r) reaches 11.5 W/m^2 (3.0 W/m^2). The differences in surface fluxes lead to the surface temperature difference, Tg_{gm} can be up to 1.52 K, with the mean deviation Tg_r of 0.29 K, and the maximum 850 hPa temperature difference $T8_{gm}$ reaches 0.24 K for a grid cell, with the mean deviation $T8_r$ of 0.05 K. This shows that the major surface characteristics are also quite sensitive to the heterogeneity in accordance with the extent of the distributed concentration of stomatal resistance. Additionally, the *Ps* values are 627 mm and 497 mm in EPT10 and EPT12, respectively, which also displays a large difference.

As we examine the HBR region, similar sensitivities can be seen (e.g., see Table 4).

It should be noted that, the sensitivities analyzed in this section are not overestimated, for instance, in EPT01 and EPT07 with different roughness-length heterogeneities, the mean surface temperatures are 297.26 K and 296.79 K for the HBR region, respectively (Table 4).

4. Summary and conclusions

In this paper, the land surface heterogeneities in roughness length and stomatal resistance, rather than those in moisture and temperature (Giorgi, 1997a), have been studied. We have employed a continuous approach (Giorgi, 1997a), which is a combination of the mosaic approach and the analytical type of the statistical-dynamical approach and is computationally efficient, to represent the heterogeneities in BATS (Dickinson et al, 1993). Different from the methodology in Giorgi (1997a), the independent variable of probability density function (PDF) is extended to the single valued function of basic meteorological characteristic quantities, which is more universal for applications. Based on this methodology, analytical expressions of characteristic quantities affected by the heterogeneities, e.g., drag coefficient, snow coverage, within-foliage windspeed and leaf surface aerodynamical resistance, are obtained. Only by computing the expressions without the use of the full land surface scheme, we have obtained some sensitivities of the quantities to the heterogeneities, e.g., the more heterogeneous roughness length, the greater differences between the characteristic quantities with and without heterogeneity treatment, and the drag coefficient seems to be most sensitive as compared to other quantities.

Previous studies of land surface heterogeneities are generally focused on off-line experiments (e.g., Entekhabi et al, 1989; Li and Avissar, 1994; Giorgi, 1997b), as is unable to represent the strong nonlinear interactions between the surface and the atmosphere. In this paper, however, coupled-model experiments have been performed with the application of a new regional climate model, which is based on the regional climate model RegCM2 (Giorgi et al, 1993a, b) and includes heterogeneity representation. The observational data of May–July, 1991 have been used as the initial and lateral boundary conditions, and the major conclusions obtained from the simulations are as follows:

(1) For the whole model domain, the consideration of the two heterogeneities greatly affects the simulations for the surface flux, wind, temperature and precipitation fields, while for different sub-regions, the extents of the influences of the heterogeneities are different. In fact, this also means the simulations for these quantities are sensitive to intrapatch heterogeneity due to the same interpatch heterogeneity initially considered. For a certain region, the heterogeneity-induced differences can amount to about 0.5 K, 0.2 K, 4 W/m^2 for the mean surface temperature, 850 hPa air temperature, sensible/latent heat flux, respectively. While for a grid cell, the differences can reach around 3 K, 0.5 K, 30 W/m^2 for the corresponding quantities, respectively.

(2) The temperature and heat fluxes are relatively sensitive to roughness-length heterogeneity, which displays the following rule: for a certain region, the mean sensible heat flux decreases, the mean latent heat flux increases, and the mean surface temperature decreases with the increase of roughness-length heterogeneity. And analogous is the rule of the effects of stomatal-resistance heterogeneity. Furthermore, our coupled-model experiments have confirmed a conclusion, i.e., the mean latent heat flux is more sensitive to the heterogeneities than the mean sensible

heat flux, obtained by use of off-line experiments in Li and Avissar (1994).

(3) It seems that the influence of the stomatal-resistance heterogeneity on the latent heat flux is greater than that of the roughness length-heterogeneity in certain cases.

From the results, it can be concluded that appropriate heterogeneity representation can improve regional climate modeling. For further investigations, we suggest that the model include other major heterogeneities (e.g., soil moisture and temperature) in addition to the heterogeneities in this study.

Appendix A

Heterogeneity treatment results of two characteristic quantities

A.1 Roughness-length heterogeneity

We also employ $f_{pdf}(y)$ as a linear PDF (Giorgi, 1997a), and assume the average, half width and height ratio of y denoted by y_0, α, γ (see Fig. A.1), respectively, then

$$f_{pdf}(y) = c_1 y + d_1, \quad \text{if} \quad y_0 - \alpha \le y \le y_0; \tag{A.1a}$$

$$f_{pdf}(y) = c_2 y + d_2, \quad \text{if} \quad y_0 \le y \le y_0 + \alpha, \tag{A.1b}$$

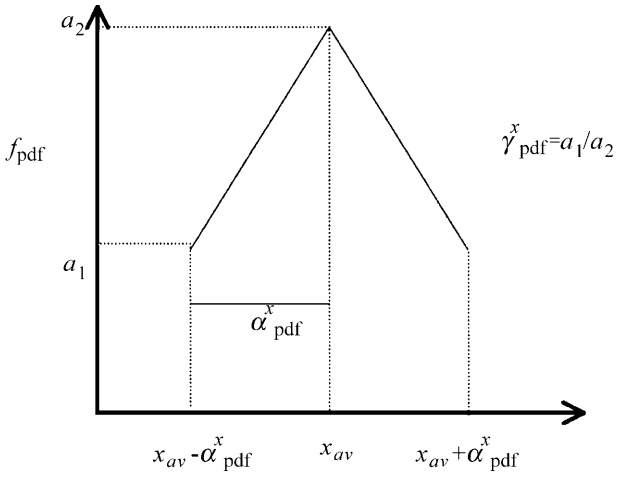

Fig. A.1. The PDF employed in Giorgi (1997a), where x_{av}, α^x_{pdf} and γ^x_{pdf} are the gridpoint average, half width, and height ratio (i.e., the ratio of a_1, the minimum, to a_2, the maximum of f_{pdf}, the PDF), respectively. In this paper, the linear PDF is also employed for y and r_s. For the distribution of y, α and γ correspond to α^x_{pdf} and γ^x_{pdf}, respectively, and for simplicity, α is replaced by α_n, width ratio that is defined as the ratio of half width to the average (i.e., α/y_0). Similar is width ratio of the PDF of r_s

where

$$\begin{aligned} c_1 &= a_2(1-\gamma)/\alpha, \quad \text{and} \\ d_1 &= a_2[\gamma + (1-\gamma)(-y_0+\alpha)/\alpha] \end{aligned} \tag{A.2a}$$

for $y_0 - \alpha \le y \le y_0$, and

$$\begin{aligned} c_2 &= -a_2(1-\gamma)/\alpha, \quad \text{and} \\ d_2 &= a_2[\gamma + (1-\gamma)y_0/\alpha] \end{aligned} \tag{A.2b}$$

for $y_0 \le y \le y_0 + \alpha$.

In (A.2), a_2 is the maximum PDF value. The treatment for C_{DN} can derived from

$$\begin{aligned} F^y_{pdf}(C_{DN}) &= \int \left[\frac{k}{y}\right]^2 f_{pdf}(y)dy \\ &= k^2 \sum_{i=1}^{2} \int \frac{c_i y + d_i}{y^2} dy \\ &= k^2 \sum_{i=1}^{2} \left(c_i \ln y - \frac{d_i}{y} \right) \Bigg|_{yi1}^{yi2}. \end{aligned} \tag{A.3}$$

The right-hand side of (A.3) consists of 8 terms, where

$$y_0 = k/\sqrt{C_{DN0}}, \tag{A.4}$$

$$y_1 = y_0 - \alpha, \; y_2 = y_0 + \alpha; \tag{A.5a}$$

$$y_{11} = y_1, \; y_{12} = y_0, \quad \text{for} \quad i = 1; \tag{A.5b}$$

$$y_{21} = y_0, \; y_{22} = y_2, \quad \text{for} \quad i = 2. \tag{A.5c}$$

In (A.4), C_{DN0} is an output from BAT0.

Since y is a single-valued function of z_0, $h_{pdf}(z_0)$, the PDF of z_0, can be obtained by

$$\begin{aligned} h_{pdf}(z_0) &= f_{pdf}[y(z_0)] \left| \frac{dy}{dz_0} \right| \\ &= \frac{\{c_i[\ln(z_1 - d_{00}z_0) - \ln z_0] + d_i\} z_1}{(z_1 - d_{00}z_0) z_0}. \end{aligned} \tag{A.6}$$

Due to effects of different land using, the realistic PDF of z_0 would be very complex, and here the derived single-peak pattern of (A.6) is applied. Besides, the average expression of z_0 can be computed from (6).

Snow coverage f_{SNOW} in BAT0 is written as

$$f_{SNOW} = Sr/(Sr + z_0), \tag{A.7}$$

where Sr is independent of z_0. Using heterogeneity operator, we obtain

$$\begin{aligned} &F^y_{pdf}(f_{SNOW}) \\ &= \sum_{i=1}^{2} \int_{z_0} \frac{Sr\{c_i[\ln(z_1 - d_{00}z_0) - \ln z_0] + d_i\}}{z_0 + Sr} \\ &\quad d[\ln(z_1 - d_{00}z_0) - \ln z_0] \\ &= \sum_{i=1}^{2} (R1 + R2 + R3 + R4), \end{aligned} \tag{A.8}$$

where

$$R1 \approx c_i d_{00} Sr/(z_1 + d_{00} Sr) \left\{ \frac{1}{2}[\ln(z_1 - d1_{00} z_0)]^2 - \ln(z_1 + d_{00} Sr)\ln(d_{00} z_1 + d_{00} Sr) + \sum_{k=1}^{4} \{(d_{00} z_1 + d_{00} Sr)/ [k(z_1 + d_{00} Sr)]\}^k \right\} \Bigg|_{zi1}^{zi2},$$

$$R2 \approx d_{00} Srd_i/(z_1 + d_{00} Sr) \left\{ \ln[(z_1 - d1_{00} z_0)/(d_{00} z_0 + d_{00} Sr)] - \frac{c_i}{d_i}[\ln(z_1/d_{00})\ln(z_1/d_{00} - z_0) + \frac{1}{2}\ln^2(z_0 + Sr)] + \frac{c_i}{d_i}\sum_{k=1}^{4}\{Sr/[k(z_0 + Sr)]\}^k - \frac{c_i}{d_i}\sum_{k=1}^{4}[(z_1 - d1_{00} z_0)/(kz_1)]^k \right\} \Bigg|_{zi1}^{zi2},$$

$$R3 = Src_i \left\{ \ln z_1 \ln z_0 - \ln(z_1 + d_{00} Sr) \ln[(z_0 + Sr)d_{00}] - \frac{1}{2}\ln^2 z_0 + \frac{1}{2}\ln^2(z_0 + Sr) \right\} \Bigg|_{zi1}^{zi2},$$

and

$$R4 \approx Srd_i \ln[z_0/(z_0 + Sr)]\Big|_{zi1}^{zi2} + Src_i \left\{ \sum_{k=1}^{4}\{Sr/[k(z_0 + Sr)]\}^k - [(d1_{00} z_0/(kz_1)]^k + [(d1_{00}(z_0 + Sr)/ [kz_1(z_1 + d_{00} Sr)]]^k \right\} \Bigg|_{zi1}^{zi2}.$$

In above terms, some mathematically complex transformations and approximations are used, e.g.,

$$\sum_{i=1}^{2}\int_{z_0}\frac{\ln(z_1 - d_{00} z_0)}{z_0 + Sr}dz_0 = \sum_{i=1}^{2}\int_{z_0}\frac{\ln[z_1 + d_{00} Sr - (d_{00} Sr + d_{00} z_0)]}{d_{00}(z_0 + Sr)}d(d_{00} Sr + d_{00} z_0)$$

$$= \sum_{i=1}^{2}\int_{z_0}\frac{\ln\{(z_1 + d_{00} Sr)[1 - (d_{00} Sr + d_{00} z_0)/(z_1 + d_{00} Sr)]\}}{d_{00}(z_0 + Sr)}d(d_{00} Sr + d_{00} z_0)$$

$$\xrightarrow[p = d_{00}(Sr + z_0)]{} \sum_{i=1}^{2}\left\{\int_p \frac{\ln(z_1 + d_{00} Sr)}{p}dp + \sum_{i=1}^{2}\int_p \frac{\ln[1 - p/(z_1 + d_{00} Sr)]}{p}dp \right.$$

$$\xrightarrow[p/(z_1 + d_{00} Sr) < 1]{\text{approximating}} \sum_{i=1}^{2}\left\{\int_p \frac{\ln(z_1 + d_{00} Sr)}{p}dp + \sum_{i=1}^{2}\int_p \sum_{k=1}^{4}\frac{-p^k/[k(z_1 + d_{00} Sr)^k]}{p}dp, \right. \quad (A.9)$$

and then, the last form of the expression allows analytical integrations.

Other quantities, such as the wind speed within the foliage layer and aerodynamical resistance at the foliage layer (Dickinson et al, 1993), are taken as simple functions of y, and the expressions after heterogeneity treatment can be easily derived (not given for the sake of paper length).

A.2 Stomatal-resistance heterogeneity

In BAT0, transpiration rate E_{tr} is calculated by

$$E_{tr} = c_g\left(\frac{1}{r_{la} + r_s}\right)(q_f^{SAT} - q_{af}), \quad (A.10)$$

where r_{la} is the aerodynamical resistance at the foliage layer, r_s the stomatal resistance, q_f^{SAT} the saturation specific humidity corresponding to the leaf temperature, q_{af} the specific humidity of the air within the foliage, and c_g a coefficient that does not vary with both r_{la} and r_s, and where r_{la} and r_s are independent of each other.

According to BAT0 formulae, it can be proved that r_{la} is approximately proportional to the square root of y:

$$r_{la} = C_E\sqrt{y}, \quad (A.11)$$

where C_E is a coefficient independent of y.

In BAT0, many factors affecting r_s are highly heterogeneous. For example, r_s has a very complicated relationship with the sky situation, solar zenith, leaf area index, etc. Avissar (1993) suggested the lognormal PDF for stomatal-conductance distribution from observed data (i.e., stomatal-resistance distribution follows the lognormal PDF), and Li and Avissar (1994) performed sensitivity experiments using 11 PDFs (e.g., normal and beta PDFs). Hence, we assume what BAT0 outputs are averages, on the basis of which the heterogeneity is considered. If we take

$$q = r_s/C_E, \quad (A.12)$$

and choose $g_{pdf}(q)$ as the linear PDF, in which c_{qj}, d_{qj}, γ_q and α_q correspond to c_i, d_i, γ and α, and in which q_j, q_0, q_{j1} and q_{j2} correspond to y_i, y_0, y_{i1} and y_{i2}. q_0 is the value of q computed by r_s and C_E, i.e., the two output values from

BAT0, via the above equation. In addition, it can be proved that the values of PDF parameters (e.g., width ratio) for q and r_s are the same.

Analogously, the corresponding heterogeneity operator is written as

$$G^q_{pdf}(A) = \int A g_{pdf}(q) dq. \tag{A.13}$$

Then the treatment of (A.7) involves that of the inverse of $(\sqrt{y} + q)$, which is represented as

$$G^q_{pdf}\{F^y_{pdf}[(r_{la} + r_s)^{-1}]\} = 2C_E \sum_{j=1}^{2}\sum_{i=1}^{2} (T1 + T2 - T3 - T4 + T5), \tag{A.14}$$

where the 5 terms are calculated by:

$$T1 = \int_q \int_x x(c_i x^2 + d_i) c_{qj} dx dq = \left(c_{qj} c_i \frac{x^4}{4} + d_i c_{qj} \frac{x^2}{2} \right) \Big|_{xi1}^{xi2} q \Big|_{qj1}^{qj2},$$

$$T2 = \ln(x + q_{j2})(Ax^5 + Bx^4 + Cx^3 + Dx^2)\Big|_{xi1}^{xi2},$$

$$T3 = \ln(x + q_{j1})(Ax^5 + Bx^4 + Cx^3 + Dx^2)\Big|_{xi1}^{xi2},$$

$$T4 = \left[\frac{As^5}{5} + \frac{(B - 5Aq_{j2})s^4}{4} + \frac{(10Aq_{j2}^2 - 4Bq_{j2} + C)s^3}{3} - \frac{(10Aq_{j2}^3 - 6Bq_{j2}^2 + 3Cq_{j2} - D)s^2}{2} + (5Aq_{j2}^4 - 4Bq_{j2}^3 + 3Cq_{j2}^2 - 2Dq_{j2})s + (-Aq_{j2}^5 + Bq_{j2}^4 - Cq_{j2}^3 + Dq_{j2}^2)\ln s \right] \Big|_{xi1+qj2}^{xi2+qj2},$$

and

$$T5 = \left[\frac{As^5}{5} + \frac{(B - 5Aq_{j1})s^4}{4} + \frac{(10Aq_{j1}^2 - 4Bq_{j1} + C)s^3}{3} - \frac{(10Aq_{j1}^3 - 6Bq_{j1}^2 + 3Cq_{j1} - D)s^2}{2} + (5Aq_{j1}^4 - 4Bq_{j1}^3 + 3Cq_{j1}^2 - 2Dq_{j1})s + (-Aq_{j1}^5 + Bq_{j1}^4 - Cq_{j1}^3 + Dq_{j1}^2)\ln s \right] \Big|_{xi1+qj1}^{xi2+qj1}.$$

(For terms $T1 - T3$, $x = y^{1/2}$; while $s = x + q_{j2}$ for $T4$ and $s = x + q_{j1}$ for $T5$).

Acknowledgements

This work is supported by the Chinese NKBRSF Project G1999043400 and the foundation of China Ministry of Education (Grant No. 20010284027). The authors would like to thank two anonymous reviewers for their comments on this work.

References

Anthes RA, Hsie EY, Kuo YH (1987) Description of the Penn State/NCAR Mesoscale Model Version 4(MM4), NCAR Tech. Note, NCAR/TN-283 + STR, National Center for Atmospheric Research, Boulder, CO

Avissar R, Pielke RA (1989) A parameterization of heterogeneous land surface for atmospheric numerical models and its impacts on regional meteorology. Mon Wea Rev 117: 2113–2136

Avissar R (1992) Conceptual aspects of a statistical-dynamical approach to represent landscape sub-grid heterogeneities in atmospheric models. J Geophys Res 97: 2729–2742

Avissar R (1993) Observations of leaf stomatal conductance at the canopy scale: An atmospheric modeling perspective. Bound-Layer Meteorol 64: 127–148

Carlson TN (1991) Modeling stomatal resistance: an overview of the 1989 workshop of the Pennsylvania State University. Agric Meteorol 54: 103–107

Dickinson RE, Henderson-Sellers A, Kennedy PJ, Wilson MF (1993) Biosphere/Atmosphere Transfer Scheme (BATS) Version 1e as Coupled to the NCAR Community Climate Model. NCAR Tech. Note TN-387 + STR, National Center for Atmospheric Research, Boulder, CO

Entekhabi D, Eagleson P (1989) Land surface hydrology parameterization for the atmospheric general models including subgrid-scale spatial variability. J Clim 2: 816–831

Giorgi F, Marinucci MR, Bates GT (1993a) Development of a second generation regional climate model (REGCM2), Boundary layer and radiative transfer processes. Mon Wea Rev 121: 2794–2813

Giorgi F, Marinucci MR, DeCanio G, Bates GT (1993b) Development of a second generation regional climate model (REGCM2), Cumulus cloud and assimilation of lateral boundary conditions. Mon Wea Rev 121: 2814–2832

Giorgi F (1997a) An approach for the representation of surface heterogeneity in land surface heterogeneity in land surface models, I: Theoretical frame work. Mon Wea Rev 125: 1885–1899

Giorgi F (1997b) An approach for the representation of surface heterogeneity in land surface heterogeneity in land surface models, II: Validation and sensitivity experiments. Mon Wea Rev 125: 1900–1919

Giorgi F, Avissar R (1997) Representation of heterogeneity effects in earth system modeling: Experience from land surface modeling. Rev Geophys 34: 413–437

Giorgi F, Mearns LO (1999) Introduction to special section: Regional climate modeling revisited. J Geophys Res 104: 6335–6352

Holtslag AAM, de Bruijn EIF, Pan HL (1990) A high resolution are mass transformation model for short range forcasting. Mon Wea Rev 118: 1561–1575

Holtslag AAM, Boville BA (1993) Local versus nonlocal boundary-layer diffusion in global climate model. J Clim 6: 1825–1842

Houlton J (1997) Global warming: The complete briefing. Cambridge, UK: Cambridge University Press, pp 18–20

Koster R, Suarez M (1992) Modeling the landsurface boundary in climate models as a composite of independent vegetation stands. J Geophys Res 97: 2697–1715

Leung LR, Ghan SJ (1995) A sub-grid parameterization of orographic precipitation. Theor Appl Climatol 52: 95–118

Leung LR, Ghan SJ (1998) Parameterizing subgrid orographic precipitation and surface cover in climate models. Mon Wea Rev 126: 3271–3291

Li B, Avissar R (1994) The impact of spatial variability of land surface characteristics on land-surface heat fluxes. J Clim 7: 527–537

Liang X, Lettenmaier DP, Wood EF (1996) One-dimensional statistical dynamic representation of subgrid spatial variability of precipitation in the two-layer variable infiltration capacity model. J Geophys Res 101: 21403–21422

Liu YQ, Weaver CP, Avissar R (1999) Toward a parameterization of mesoscale fluxes and moist convection induced by landscape heterogeneity. J Geophys Res 104: 19515–19533

Olson JS, Watts JA, Allison LJ (1983) Carbon in live vegetation of major world ecosystems. U.S. Department of Energy, DOE/NBB-0037, No.TR004, U.S. Department of Energy, Washington, DC, 152pp

Pitman AJ, Henderson-Sellers A, Yang ZL (1990) Sensitivity of regional climates to localized precipitation in global models. Nature 346: 734–737

Seth A, Giorgi F, Dickinson RE (1994) Simulating fluxes from heterogeneous land surfaces: Explicit sub-grid method employing the Biosphere/Atmosphere Transfer Scheme (BATS). J Geophys Res 99: 18561–18667

Sivapalan M, Woods RA (1995) Evaluation of the effects of general circulation model's sub-grid variability and patchiness of rainfall and soil moisture on land surface water balance fluxes. In: Scale issues in hydrological modeling (Kalma JD, Sivapalan M, eds) New York, Wiley, pp 453–473

Walko RL, Band LE, Baron J et al (2000) Coupled atmosphere-biophysics-hydrology models for environmental modeling. J Appl Meteor 39: 931–944

Wang GL, Eltahir EAB (2000) Modeling the biosphere-atmosphere system: The impact of the subgrid variability in rainfall interception. J Clim 13 2887–2899

Corresponding author's address: Xin-Min Zeng, Department of Atmospheric Sciences, Nanjing University, Nanjing 210093, P. R. China (E-mail: zen_xm@yahoo.com)